OPEN ACCESS
Journal of Innovative Optical Health Sciences
Vol. 16, No. 1 (2023) 2245005 (12 pages)

DOI: 10.1142/S1793545822450055

World Scientific
www.worldscientific.com

Fluorescence imaging analysis of the glioma microenvironment

Xuwen Peng, Yuzhou Chen, Yuke Wang and Shuhong Qi*
Britton Chance Center for Biomedical Photonics
Wuhan National Laboratory for
Optoelectronics-Huazhong
University of Science and Technology
Wuhan, Hubei 430074, P. R. China

MoE Key Laboratory for Biomedical Photonics
School of Engineering Sciences
Huazhong University of Science and Technology
Wuhan, Hubei 430074, P. R. China
**qishuhong@hust.edu.cn*

Received 28 September 2022
Accepted 14 December 2022
Published 6 February 2023

Glioma is the most malignant brain cancer. The neurons, macrophages, T cells and other immune cells constitute the glioma immunosuppressive microenvironment. The accurate spatial distribution of these cells in the glioma microenvironment and its relationship with glioma metastasis is unknown. We constructed a mouse glioma cell line stably expressing the large Stokes-shifted yellow fluorescent protein and applied it to the multicolor immunofluorescence imaging. The imaging data revealed that the neurons were sparsely distributed in the glioma core and the number of neurons decreased by 90% compared with normal brain site. The spatial distribution of monocyte-macrophages and microglia is heterogeneous. The monocyte-macrophages and T cells were heavily recruited into the glioma core and metastasis. There was no significant difference in the distribution of microglia among glioma core, margin, and normal brain site. Our results provided new perspectives for targeting immune regulation cells and developing new immunotherapy strategies for glioma.

Keywords: Glioma microenvironment; spatial distribution; heterogeneity; multicolor immunofluorescence; large Stokes-shifted fluorescent protein.

*Corresponding author.

1. Introduction

Glioma is the most aggressive brain cancer with poor survival and high recurrence.[1–3] The glioma microenvironment is complex, consisting of neurons, microvascular, astrocytes, and various immune cells, such as microglia, monocyte-macrophages, and T lymphocytes.[4–6] These components play important roles in the process of glioma invasion and metastasis.[7,8]

Neurons are a crucial component of the glioma microenvironment. Growing evidence has shown that the bidirectional communication existing between neurons and glioma cells regulates malignant glioma progression.[9–12] Glioma cells can create electrical synapses with surrounding neurons, which drives glioma growth and migration.[12] Meanwhile, the invasion of glioma cells into surrounding brain parenchyma significantly reduces the number of inhibitory interneurons.[9,13–15] The decrease of inhibitory interneurons renders peritumoral neuronal networks hyper-excitable, and the excitatory stimuli enhanced the invasion of glioma cells.[9,16] In addition, as the concentration of glutamate secreted by glioma increases, it triggers the death of excitotoxic neurons and promotes the glioma proliferation and invasion.[17] Visualizing the distribution of neurons in the glioma microenvironment could expand the study of neuron-glioma spatial communications.

Glioma has a unique immunosuppressive microenvironment[18] in which glioma-associated macrophages (GAMs) are the most numerous populations.[19] GAMs consist of brain-resident microglia and peripheral blood monocyte-derived macrophages, where both participate in the formation of the immunosuppressive microenvironment and promote the development and invasion of glioma.[20] As glioma develops, the density of GAMs increases and the number of infiltrating GAMs correlates with the malignancy of glioma.[21,22] GAMs also inhibit the activity of cytotoxic T lymphocytes and induce infiltration of regulatory T cells in the glioma microenvironment to promote immunosuppression.[23–25] T lymphocytes have also been reported to be closely associated with the prognosis of glioma patients, such as a high level of $CD4^+$ T cells and a low level of $CD8^+$ T cells were associated with poor prognosis.[26] Previous studies revealed that microglia and monocyte-macrophages have distinct functions in glioma. For example, microglia rather than monocyte-macrophages played a central role in the regulation of vascular homeostasis and angiogenesis in glioma.[27,28] To explore the heterogeneity between microglia and monocyte-macrophages, the scientists used two-photon intravital imaging to investigate their morphology and motility. The imaging results showed that microglia were larger, more branched and less motile, while

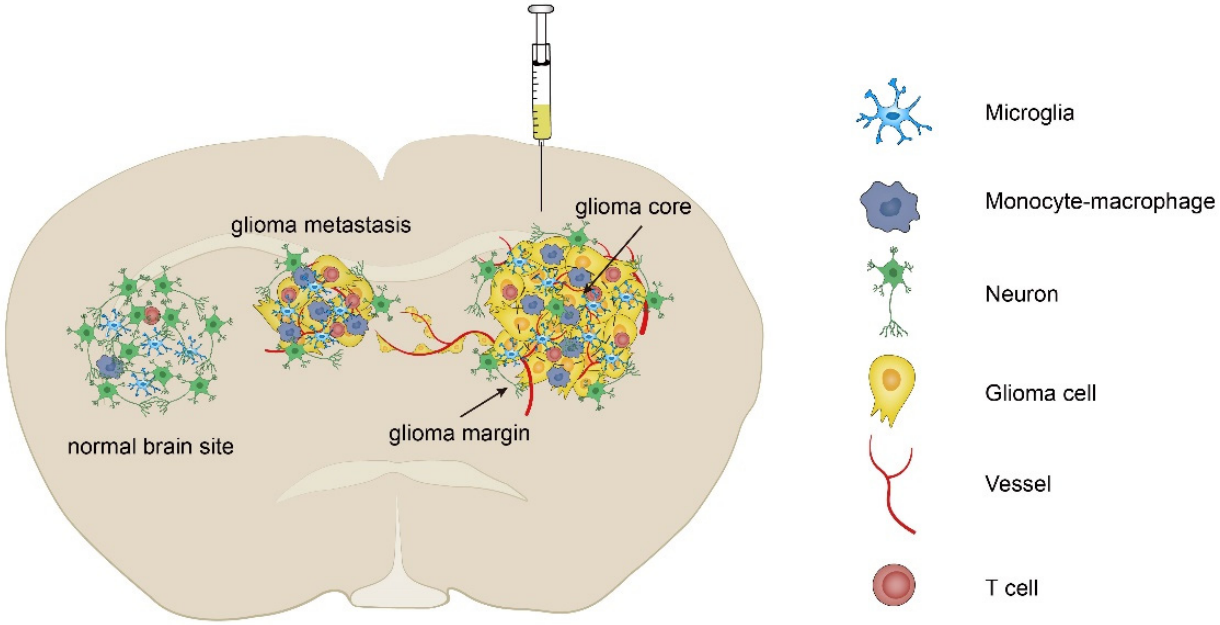

Scheme 1. Components of the glioma microenvironment.

monocyte-macrophages were smaller, less branched and highly migratory.[29] However, the spatial distribution heterogeneity between microglia and monocyte-macrophages is not well known. Therefore, studying the spatial distribution of microglia, monocyte-macrophages and T cell in the glioma microenvironment, as well as metastasis, will contribute to understanding the mechanisms of glioma development and metastasis.

In recent years, multicolor immunofluorescence has been widely used, which meets the needs of histological analysis and can achieve rich information from the simultaneous detection of multiple target molecules at the same time on the same tissue section.[30,31] Currently, the scientists used multicolor immunofluorescence to reveal that in the glioma recurrence microenvironment, the increased signaling interaction between neoplastic cells and neighboring neural cells facilitated greater glioma invasion into the normal brain.[32] Another study applied multicolor immunofluorescence to provide a comprehensive immune cell landscape describing the changes in cellular state from normal tissue to glioma.[33] Thus, we adopted multicolor immunofluorescence techniques to explore and analyze the glioma microenvironment and metastasis to obtain quantitative information on the spatial distribution of neurons and multiple immune cells.

In this study, we screened a mouse glioma GL261 cell line stably expressing the large Stokes-shifted yellow fluorescent protein mAmetrine (named mAmetrine-GL261). By using multicolor immunofluorescence, we visualized the spatial distribution of neurons, microglia, monocyte-macrophages, and T cells in the mAmetrine-GL261 glioma microenvironment and metastasis (Scheme 1). As shown in Scheme 1, we found that only a few neurons were retained in the glioma core and the density of neurons in the glioma core decreased by 90% compared to the normal brain site. Imaging results illustrated that the heterogeneity existed in the spatial distribution between the microglia and monocyte-macrophages. The density of monocyte-macrophages significantly increased in the glioma core compared with normal brain site. There was no significant difference in the number of microglia in the glioma versus the normal brain site. Glioma cells have a characteristic infiltrative growth along the outer wall of blood vessels. The glioma metastasis recruited large numbers of monocyte-macrophages and T cells. These findings provide new insight into studying the aggressive growth and metastasis of glioma and are useful to design new immunotherapy strategies by targeting immunomodulation cells in the glioma.

2. Materials and Methods

2.1. *Mice*

C57BL/6 female mice were obtained from the Hunan SJA Laboratory Animal Co., Ltd (Hunan, China). B6.129P2(Cg)-$Cx_3CR_1^{tm1Litt}$/J ($CX_3CR_1^{+/gfp}$, JAX: 005582) mice were derived from breeding pairs that were obtained originally from the Jackson Laboratory (Bar Harbor, ME, USA). All the mice were bred and maintained in a specific pathogen-free (SPF) barrier facility at the Animal Center of Wuhan National Laboratory for Optoelectronics. All animal studies were approved by the Hubei Provincial Animal Care and Use Committee and followed the experimental guidelines of the Animal Experimentation Ethics Committee of the Huazhong University of Science and Technology.

2.2. *Screening mAmetrine-GL261 cell lines*

After transformation of the pB-mAmetrine plasmid and PBase plasmid into *E.coli*, the bacterial solution was spread evenly in Luria-Bertani (LB) agar (Sinopharm Chemical Reagent Co., Ltd., China) bacterial medium and incubated overnight at 37°C. A monoclonal colony in the dish was picked and placed in a conical flask with LB broth and incubated in a constant temperature shaker at 37°C and 180 rpm overnight. The pB-mAmetrine plasmid and PBase plasmid were extracted according to the instructions in the endofree plasmid midi kit (Jiangsu Cowin Biotech Co., Ltd., China) after the bacterial solution in the conical flask became turbid, and the plasmid concentration was measured using an ultra-micro spectrophotometer (ThermoFisher, USA). Then, transfection of plasmids was performed according to the instructions in the Lipofectamine 2000 Transfection Kit (ThermoFisher, USA). The fluorescence of GL261 cells in 96-well plates transfected with pB-mAmetrine plasmid as described above was observed daily using an IX71 inverted fluorescence microscope (Olympus, Japan), and GL261 cells stably expressing yellow fluorescent protein were screened by the limited dilution method.

2.3. *Stereotaxic intracranial glioma implantation*

The mice were deeply anesthetized with Avertin (Sigma, Germany) and positioned on a stereotactic frame. The head was secured using a nose clamp and two ear bars. The mouse was placed under a stereomicroscope to ensure precise surgical manipulation. The head was shaved and the skin was cut. The periosteum was scraped and a circular hole was drilled over the right parietal bone. Next, 10^4 mAmetrine-GL261 cells suspended in 4 μL of PBS were injected stereotactically using a 10 μL syringe with a 34G needle (WPI, USA) in the middle of the craniotomy at a depth of 3 mm. The exposed brain was sealed with silicone oil (Sigma-Aldrich, USA). After cell injection, the mice were sutured with surgical sutures. Finally, the mice were placed on a heating pad to maintain their body temperature until they woke up, and the mice were put back into the animal room after surgery. Mice were closely monitored twice per week for behavior, reactivity, and appearance.

2.4. *Confocal imaging*

The screened mAmetrine-GL261 cells were cultured in 25 cm^2 culture flasks and digested with trypsin when the cell density was 90% of the flask bottom. After taking the cell suspension for live cell counting, the cell suspension was diluted to 1×10^6 cells/mL using DMEM complete medium. Then, 100 μL of mAmetrine-GL261 cell suspension was added to the confocal culture dishes and spread evenly and incubated at 37°C in a 5% CO_2 cell incubator. The LSM 710 laser confocal microscope (Zeiss, Germany) was used to image the cells when the cells were spread over 80% of the laser confocal culture dish. The excitation peak wavelength of yellow fluorescent protein mAmetrine is 406 nm and the emission peak wavelength is 526 nm. Therefore, the excitation wavelength of the LSM 710 laser confocal microscope was set to 405 nm, and the detection wavelength of the detection channel was set to 504–563 nm. The fluorescence and bright field were imaged simultaneously to observe the fluorescent protein expression of mAmetrine-GL261 cells.

2.5. *Flow cytometry*

Two groups of GL261 cells without fluorescent protein expression and mAmetrine-GL261 cells were established. They are Culture GL261 and mAmetrine-GL261 cells. When the density is 90% of the bottom of the 25 cm^2 cell culture flask, aspirate the GL261 and mAmetrine-GL261 cell suspensions (200 μL). Add eBioscience™ Fixable Viability Dye to the cell suspension in the EP tube, dilute the dye in the final cell suspension by 1000x and incubate on ice in a dark place for 30 min. After the incubation is complete, add 2 mL of PBS containing 2% NCS to the centrifuge tube, set the centrifuge parameters to 4°C, 500 g, and centrifuge for 5 min. Discard the supernatant and resuspend the cells using 200 μL of 2% NCS-containing PBS for flow cytometry.[34] Use nonfluorescent GL261 cells as a negative control for fluorescence signal, and subsequently detect the fluorescence signal of mAmetrine-GL261 cells under the same flow cytometry parameters.

2.6. *Glioma staining in vivo*

Mice were intracranially inoculated with mAmetrine-GL261. On day 25 of glioma growth, animals were injected via tail vein with 60 mg/kg Evans Blue in sterile saline solution. Mice were anesthetized and perfused with the heart 60 min later. Then, mice were euthanized and brains were removed and preserved in 4% PFA. After fixation was completed, the whole brain of the mice was cut along the coronal plane to observe the Evans Blue staining.

2.7. *Immunofluorescence and histopathology*

Mice were intracranially inoculated with mAmetrine-GL261. On day 25, mice were perfused with the heart. The brains were removed intact, fixed overnight in 4% PFA, and then dehydrated in a gradient. After the brain tissue had sunk to the bottom, it was embedded in the Tissue-Tek OCT compound and sectioned into 20 μm slices on a Leica CM1950 cryostat (Wetzlar, Germany) at −20°C. The anti-NeuN antibody EPR12763 (1:800, ab177487, Abcam, Cambridge, USA) and the goat anti-rabbit IgG H&L Alexa Fluor 488 (1:1000, ab150077, Abcam, USA) were used to identify neurons in the brain. The anti-CD31 antibody (1:50, ab28364, Abcam, USA) and the goat anti-rabbit IgG H&L Alexa Fluor 488 (1:1000, ab150077, Abcam, USA) were used to mark vessels. Brilliant Violet 421™ anti-mouse F4/80

(1:100, 565411, BD Biosciences, USA) was used to recognize macrophages. Anti-mouse CD3 antibody Alexa Fluor 594 (1:200, 100240, BioLegend, USA) was used to identify the T cells. All brain slices were imaged on a Zeiss LSM 710 laser scanning confocal microscopy (Oberkochen, Germany). The data were analyzed with ImageJ (NIH, USA).

For histopathology, fixed brain tissues were embedded in paraffin, sectioned, and stained with hematoxylin–eosin (H&E). The H&E slices were imaged on a Nikon Ni-E microscope (Nikon, Minato, Tokyo, Japan). All images were analyzed with ImageJ (NIH, USA).

2.8. *Statistical analysis*

Statistical analysis was performed using GraphPad Prism 7 (GraphPad Software, Inc., La Jolla, CA, USA). For comparisons of two groups, the two-tailed unpaired *t*-test or Mann–Whitney test was used. For comparisons of three groups, the one-way ANOVA with Tukey's multiple comparison test or Kruskal–Wallis test was used. The statistical analysis is described in each figure legend. Differences between or among groups are denoted as ns for not significant, * for $P < 0.05$, ** for $P < 0.01$, *** for $P < 0.001$ and **** for $P < 0.0001$.

3. Results and Discussion

3.1. *Screening GL261 cells with stable expression of mAmetrine*

The mouse glioma GL261 cells were transfected with the PB transport system, which contained the sequence encoding a large Stokes-shifted yellow fluorescent protein (named mAmetrine) to generate the mAmetrine-GL261 cell line. The mAmetrine is a yellow fluorescent protein with a large Stokes shift (with an excitation wavelength of 406 nm, an emission wavelength of 526 nm, and a Stokes shift of 120 nm),[35] considerably reducing the overlap between the excitation and emission spectra. It can effectively reduce the crosstalk of fluorescence spectra, and avoid fluorescence efficiency reduction caused by energy transfer.[36] To assess whether GL261 cells stably express mAmetrine, we used laser confocal microscopy to image the mAmetrine-GL261 cells (Fig. 1(a)). Confocal imaging showed that the percentage of fluorescent cells was more than 95% (Fig. 1(b)).

Next, we examined the percentage of GL261 cells stably expressing mAmetrine in total cells. The positive cell population was segregated from the negative cell population, and the mean fluorescence intensity of mAmetrine-GL261 cells was 1321-fold

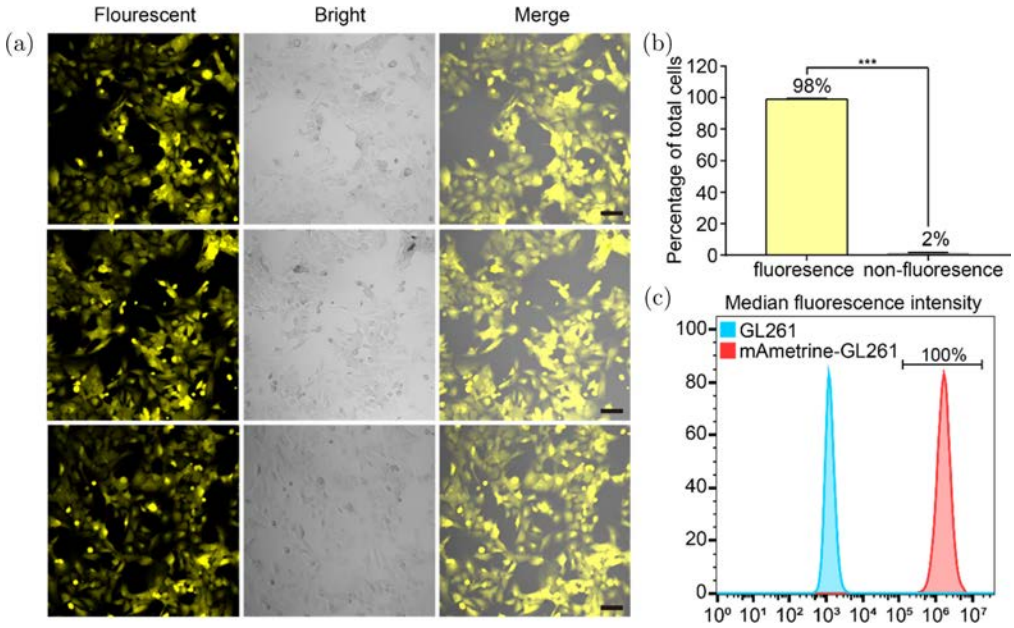

Fig. 1. The detection of mAmetrine-GL261 cells. (a) Representative confocal images of mAemtrine-GL261. (b) Statistics of fluorescent and nonfluorescent cells in 11 images. (Three independent experiments). (c) The median fluorescence intensity of GL261 and mAmetrine-GL261. Statistical analysis was performed using the two-tailed unpaired *t*-test. The data were present as mean ± SD. ***$P < 0.001$.

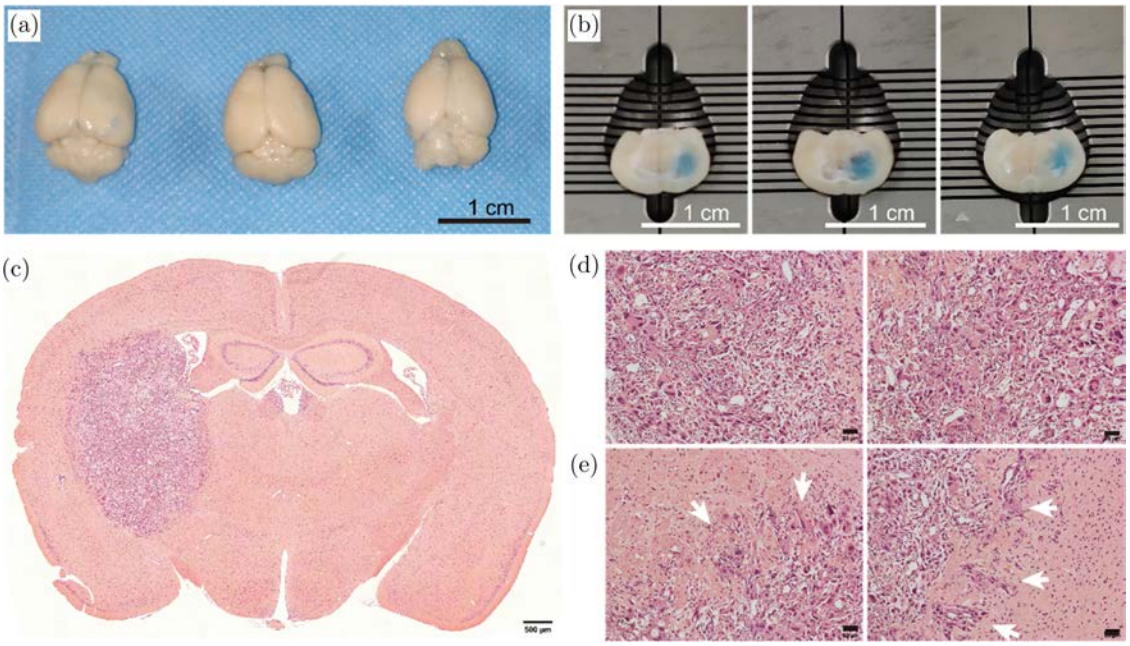

Fig. 2. Staining results of mice brains on day 25 after mAmetrine-GL261 cells implantation. (a) Evans Blue staining of the mouse brain surface. Scale bar: 1 cm. (b) Evans Blue staining of mouse deep brain. Scale bar: 1 cm. (c) H&E staining results of the whole brain. Scale bar: 500 μm. (d) Glioma core. Scale bar: 50 μm. (e) Glioma margin. White arrows indicate infiltrating glioma cells. Scale bar: 50 μm.

higher than that of GL261 cells (Fig. 1(c)). The flow cytometry results confirmed that the percentage of the mAmetrine-GL261 cells with mAmetrine fluorescent signal was above 95%, which was consistent with the confocal imaging data.

This mAmetrine-GL261 cell line is suitable for multi-color fluorescence imaging. For example, the mAmetrine can be used in association with CFP (Ex: 405 nm/Em: 485 nm), GFP (Ex: 488 nm/Em: 507 nm) and mCherry (Ex: 587 nm/Em: 610 nm). Then, we detected the tumorigenicity and used mAmetrine-GL261 glioma cells in combination with immunofluorescence to provide visualization of the distribution of neurons and immune cells in the glioma microenvironment and metastasis.

3.2. *Detection of the tumorigenicity of mAmetrine-GL261 cells*

To determine whether the mAmetrine-GL261 cells could form the glioma, C57BL/6 mice were inoculated intracranially into the striatum with mAmetrine-GL261 cells and were allowed to establish gliomas for 25 days. We used Evans Blue staining to visualize the glioma area through tail vein injection, and then removed the mouse brain. The results showed that mAmetrine-GL261 cells had not yet reached the surface of the brain (Fig. 2(a)), and the region of the glioma had been stained (Fig. 2(b)), which suggested that the mAmetrine-GL261 cells could form glioma.

In addition, the mouse brain slices were prepared by H&E staining and imaged. Imaging results indicated that mAmetrine-GL261 cells were tumorigenic (Fig. 2(c)). Glioma cells grow densely in the glioma core (Fig. 2(d)). As shown by the white arrow, in the glioma margin, mAmetrine-GL261 cells infiltrated the surrounding tissues (Fig. 2(e)). Evans Blue staining and H&E staining results confirmed the tumorigenicity of the mAmetrine-GL261 cells and the growth of mAmetrine-GL261 cells was very aggressive.

3.3. *Immunofluorescence imaging of neurons in the glioma microenvironment*

To investigate the spatial distribution of neurons within the glioma microenvironment, we used the antibody Anti-NeuN (Alexa Flour 488) to label the nucleus of neurons and used confocal imaging to observe the brain slices (Figs. 3(a)–3(c)).

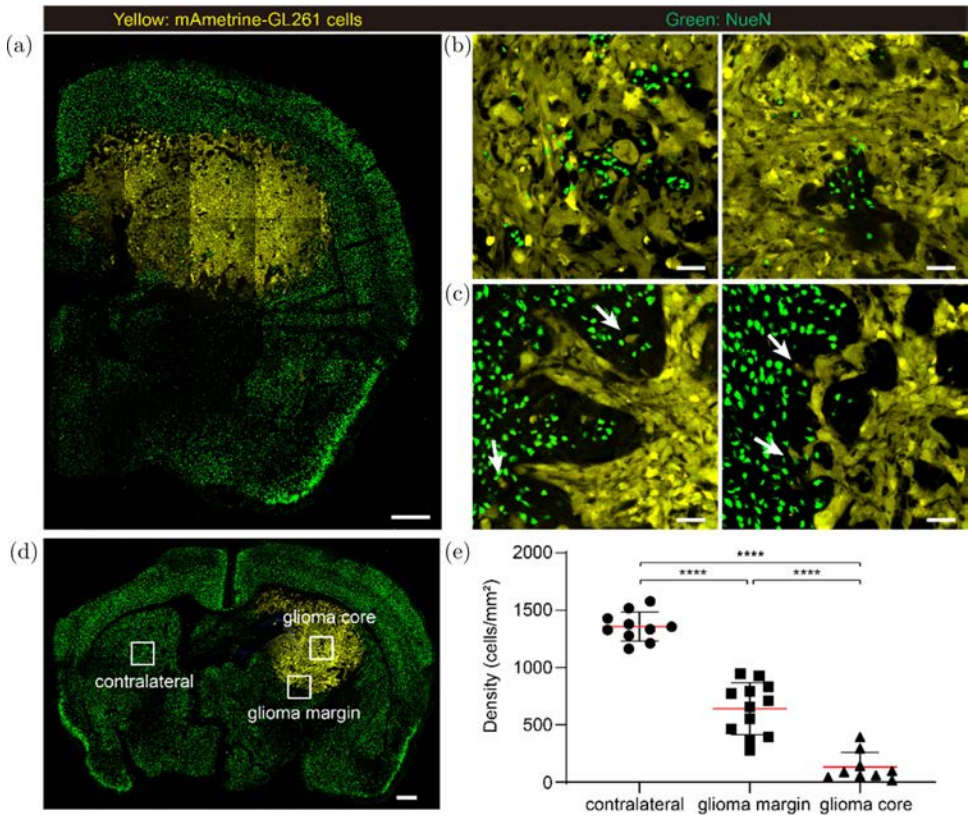

Fig. 3. Immunofluorescence imaging of brain slice on day 25 after mAmetrine-GL261 implantation. (a) Large-field of image. Scale bar: 500 μm. (b) Neuron distribution in the glioma core. Scale bar: 50 μm. (c) Neuron distribution in glioma margin. White arrows show some individual invasive glioma cells around the glioma. Scale bar: 50 μm. (d) Random imaging of the contralateral hemisphere, glioma margin and glioma core. Scale bar: 500 μm. (e) Quantitative analysis of the density of neurons in contralateral hemisphere ($n = 10$ images), glioma margin ($n = 12$ images) and glioma core ($n = 9$ images). Statistical analysis was performed using the one-way ANOVA with Tukey's multiple comparison test. The data are presented as the mean $\pm$ SD. $^{****}P < 0.0001$.

The imaging data showed that neurons were sparsely distributed in the glioma core where mAmetrine-GL261 cells grew densely. In the glioma margin, more neurons were distributed along the perimeter of the glioma while neurons were densely distributed in the normal brain site (contralateral hemisphere). In addition, we found infiltrative growth of mAmetrine-GL261 cells, and the invasion of individual glioma cells could be observed, as shown by the white arrows (Fig. 3(c)).

To quantify the distribution of neurons in the glioma core, glioma margin, and normal brain site (contralateral hemisphere), we randomly imaged several views (Fig. 3(d)). Quantitative data showed that the average density of neurons in the tumor core decreased by 90% and 50% compared to the contralateral hemisphere and glioma margin, respectively (Fig. 3(e)). The results demonstrated that the growth of glioma in the brain leads to neuronal decrease in the glioma area.

It has been demonstrated that neurons play a key role in the glioma microenvironment, which could regulate the glioma progression.[9–12] The imaging results showed that the neurons sporadically distributed in the glioma core. The reduced neurons may include inhibitory interneurons[9] and excitatory neurons[17] both of which result in the invasion of glioma cells into surrounding brain parenchyma. Therefore, designing a therapy that inhibits glioma-induced neuronal apoptosis and increases the number of neurons may contribute to glioma therapy.

3.4. *Immunofluorescence imaging of immune cells in the glioma microenvironment*

To quantify the level of infiltration and spatial distribution of immune cells in the glioma microenvironment, we used the mouse brain slices to

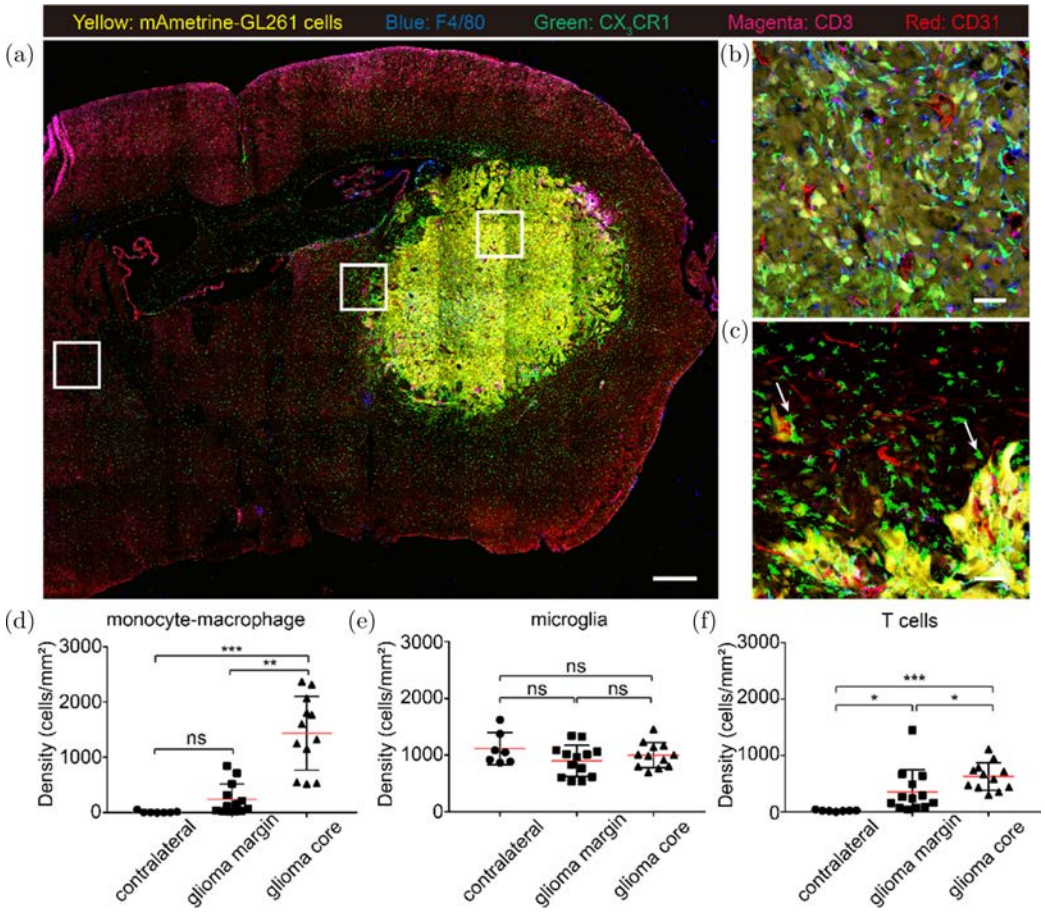

Fig. 4. Multicolor immunofluorescence imaging of the glioma microenvironment and quantitative analysis of the infiltration density and distribution of each immune cell in the glioma microenvironment. (a) Large-field of brain slice image. Scale bar: 500 μm. (b) Representative confocal microscopy images of the glioma core. Scale bar: 50 μm. (c) Representative confocal microscopy images of the glioma margin. White arrows indicate microglia. Scale bar: 50 μm. (d) The cell density of monocyte-macrophages in the glioma core, glioma margin, and normal brain site. (e) The cell density of microglia in the glioma core, glioma margin, and normal brain site. (f) The cell density of T cells in the glioma core, glioma margin, and normal brain site. The images were from three mice. Statistical analysis was performed using Kruskal–Wallis test in (d) and (f). Statistical analysis was performed using the one-way ANOVA with Tukey's multiple comparison test in (e). The data are presented as the mean $\pm$ SD. $^{*}P < 0.05$, $^{**}P < 0.01$, $^{***}P < 0.001$, and ns denotes not significant.

observe the glioma microenvironment and quantified the number of infiltrating monocyte-macrophages, microglia, and T cells in each imaging field, as shown in the white boxes (Figs. 4(a)–4(c)). We distinguished microglia from monocyte-macrophages by utilizing CX_3CR_1 mice in combination with F4/80 antibody. In the brain slice of CX_3CR_1 mice, the GFP-labeled cells were microglia, and the F4/80 antibody labeled cells were monocyte-macrophages. Compared with the contralateral hemisphere and glioma margin, the density of monocyte-macrophages was 116-fold and 6-fold higher in the glioma core, respectively (Fig. 4(d)). This indicated that monocyte-macrophages were heavily recruited to the glioma area during the growth of glioma, and the quantitative data suggested that monocyte-macrophages were mainly distributed inside the glioma. Besides, there was no significant difference in the number of microglia in these three regions, indicating that the glioma growth did not have a significant effect on the distribution of microglia in the brain (Fig. 4(e)). At the same time, imaging revealed that around the glioma, microglia were tightly recruited around the infiltrating glioma cells, indicating an interaction between the microglia and glioma cells (Fig. 4(c)).

The infiltration of $CD3^+$ T cells was similar to that of monocyte-macrophages. Compared with the normal brain site and glioma margin, the density of

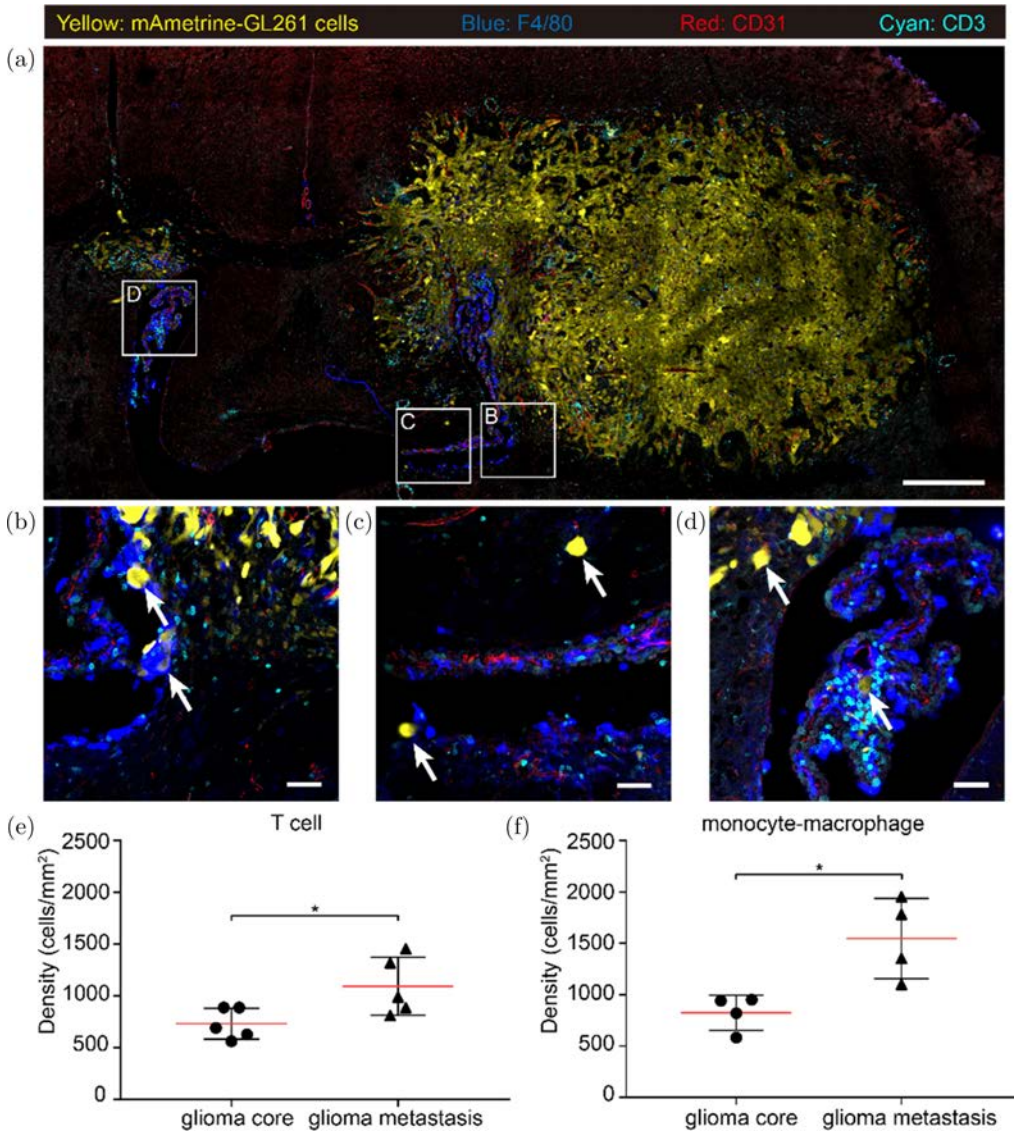

Fig. 5. Multicolor immunofluorescence imaging and quantitative analysis of glioma in the metastatic process. (a) Large-field of image of monocyte-macrophages and T cells in the *in-situ* glioma and metastasis. Scale bar: 500 μm. (b)–(d) Infiltration of T cells and monocyte-macrophages in the metastasis, white arrows indicated individual glioma cells. Scale bar: 50 μm (e) Quantitative analysis of the cell density of T cells of *in-situ* gliomas, and glioma metastasis. (F) Quantitative analysis of the monocyte-macrophage cell density of *in-situ* gliomas and glioma metastasis. Statistical analysis was performed using the unpaired student t test. ($n = 4-5$ images, from 2 to 3 mice). Data are presented as the mean $\pm$ SD. $^*P < 0.05$.

T cells inside the glioma was 30-fold and 1.8-fold higher, respectively (Fig. 4(f)). This finding indicated that $CD3^+$ T cells were largely recruited to the glioma area in large numbers during glioma development, and the quantitative data suggested that $CD3^+$ T cells were mainly distributed inside the glioma.

The imaging results showed that the distribution of monocyte-macrophages, microglia and T cells in the glioma microenvironment was spatially heterogeneous, with monocyte-macrophages and T cells mainly distributed inside the glioma, and the distribution of microglia did not have significant difference in the glioma core, glioma margin and normal brain site. The possible reason for this is that under physiological conditions, monocyte-macrophages are unable to cross the blood–brain barrier. However, as glioma developed, the blood–brain barrier is disrupted and monocyte-macrophages are recruited into the glioma microenvironment.[37] These results suggest that targeting drugs to inhibit monocyte-macrophage recruitment into the glioma region might

hinder glioma growth. The imaging study about the distinct spatial distribution between microglia and monocyte-macrophages in the glioma and metastasis could promote the discovery of distinct functions for GAMs in the glioma and facilitate developing novel immunotherapy.

3.5. *Immunofluorescence imaging of monocyte-macrophages and T cells in the glioma metastasis*

To investigate the distribution of immune cells in the glioma metastases, we imaged the mouse brain slice in which glioma metastasis occurred (Figs. 5(a)–5(d)) and observed the presence of individual glioma cells tightly surrounded by monocyte-macrophages in different regions of the mouse brain, as indicated by the white arrows (Figs. 5(b)–5(d)). It is suggested that glioma cells may have metastasized along the ventricles. In addition, we found that glioma cells invaded and grew along the outer wall of blood vessels, and we observed that glioma cells were tightly attached to the outer wall of blood vessels (Figs. 5(a)–5(d)).

We randomly imaged several fields of view within the *in-situ* glioma as well as the metastasis to quantitatively compare the density. The cell density of T cells in the glioma metastasis was approximately 1.5-fold higher than the density of T cells in the *in-situ* glioma (Fig. 5(e)). The cell density of monocyte-macrophages in the metastasis was about 1.7-fold higher than the density of monocyte-macrophages in the *in-situ* glioma (Fig. 5(f)).

The above results indicated that a large number of monocyte-macrophages and T cells are recruited into the metastasis, which further promotes the development of glioma metastasis. Previous studies have shown that monocyte-macrophages can release cytokines including IL-6 that stimulated glioma growth and invasion by acting on glioma initiating cells in the perivascular niche.[38,39] The distribution of T cells in glioma metastasis and the mechanism of their recruitment have not been reported, but the phenomenon of the elevated density of monocyte-macrophages and T cells in glioma metastasis suggests that we can develop fluorescent probes or nanodrugs targeting monocyte-macrophages or T cells, which are expected to enable sensitive diagnostic methods and immunotherapy for glioma metastasis.

4. Conclusion

In this study, we used the mAmetrine-GL261 cells combined with multicolor immunofluorescence imaging to explore the spatial distribution of neurons, monocyte-macrophages, microglia, and T cells in the glioma microenvironment. Neurons are sparsely distributed in the glioma core and the density of them was decreased by 90% compared with normal brain site. We observed the heterogeneity of spatial distribution between microglia and monocyte macrophages. Compared with normal brain site, the number of monocyte-macrophages was significantly increased in the glioma core. However, the distribution of microglia did not have a significant difference in the glioma core, glioma margin, and normal brain site. Glioma cells grew invasively along the outer wall of blood vessels. Monocyte-macrophages and T cells were abundantly recruited into the glioma metastasis. This study reveals the spatial distribution of neurons and important immune cells in the glioma microenvironment and provides a new perspective for developing immunotherapy strategies for targeting the key immune cells in the glioma.

Conflict of Interest

The authors declare that there are no conflicts of interest regarding the publication of this paper.

Acknowledgments

We thank the Optical Bioimaging Core Facility of WNLO-HUST and the Research Core Facilities for Life Science (HUST) for the support in data acquisition. We thank Prof. Xiaohui Wu from Fudan University for providing the PB transposon system and Prof. Zhihong Zhang for paper discussions. This work was supported by the National Natural Science Foundation of China (31700808) and the Fundamental Research Funds for the Central Universities (2020kfyXJJS112). Xuwen Peng and Yuzhou Chen contributed equally to this work.

References

1. M. Weller, W. Wick, K. Aldape, M. Brada, M. Berger, S. M. Pfister, R. Nishikawa, M. Rosenthal,

P. Y. Wen, R. Stupp, G. Reifenberger, "Glioma," *Nat. Rev. Dis. Prim.* **1**, 15017 (2015).
2. D. N. Louis, A. Perry, P. Wesseling, D. J. Brat, I. A. Cree, D. Figarella-Branger, C. Hawkins, H. K. Ng, S. M. Pfister, G. Reifenberger, R. Soffietti, A. von Deimling, D. W. Ellison, "The 2021 WHO Classification of Gliomas of the Central Nervous System: A summary," *Neuro Oncol.* **23**, 1231–1251 (2021).
3. A. Abdurashitov, V. Tuchin, O. Semyachkina-Glushkovskaya, "Photodynamic therapy of brain tumors and novel optical coherence tomography strategies for in vivo monitoring of cerebral fluid dynamics," *J. Innov. Opt. Health Sci.* **13**, 2030004 (2020).
4. D. F. Quail, J. A. Joyce, "The microenvironmental landscape of brain tumors," *Cancer Cell* **31**, 326–341 (2017).
5. A. Gieryng, D. Pszczolkowska, K. A. Walentynowicz, W. D. Rajan, B. Kaminska, "Immune microenvironment of gliomas," *Lab Invest* **97**, 498–518 (2017).
6. B. M. Andersen, C. Faust Akl, M. A. Wheeler, E. A. Chiocca, D. A. Reardon, F. J. Quintana, "Glial and myeloid heterogeneity in the brain tumour microenvironment," *Nat. Rev. Cancer* **21**, 786–802 (2021).
7. A. Vollmann-Zwerenz, V. Leidgens, G. Feliciello, C. A. Klein, P. Hau, "Tumor cell invasion in glioblastoma," *Int. J. Mol. Sci.* **21**, 1932 (2020).
8. S. Tamai, T. Ichinose, T. Tsutsui, S. Tanaka, F. Garaeva, H. Sabit, M. Nakada, "Tumor microenvironment in glioma invasion," *Brain Sci.* **12**, 505 (2022).
9. H. S. Venkatesh, W. Morishita, A. C. Geraghty, D. Silverbush, S. M. Gillespie, M. Arzt, L. T. Tam, C. Espenel, A. Ponnuswami, L. J. Ni, P. J. Woo, K. R. Taylor, A. Agarwal, A. Regev, D. Brang, H. Vogel, S. Hervey-Jumper, D. E. Bergles, M. L. Suva, R. C. Malenka, M. Monje, "Electrical and synaptic integration of glioma into neural circuits," *Nature* **573**, 539–545 (2019).
10. H. S. Venkatesh, T. B. Johung, V. Caretti, A. Noll, Y. J. Tang, S. Nagaraja, E. M. Gibson, C. W. Mount, J. Polepalli, S. S. Mitra, P. J. Woo, R. C. Malenka, H. Vogel, M. Bredel, P. Mallick, M. Monje, "Neuronal activity promotes glioma growth through neuroligin-3 secretion," *Cell* **161**, 803–816 (2015).
11. G. Sprugnoli, A. J. Golby, E. Santarnecchi, "Newly discovered neuron-to-glioma communication: New noninvasive therapeutic opportunities on the horizon?" *Neurooncol. Adv.* **3**, vdab018 (2021).
12. H. S. Venkatesh, L. T. Tam, P. J. Woo, J. Lennon, S. Nagaraja, S. M. Gillespie, J. Ni, D. Y. Duveau, P. J. Morris, J. J. Zhao, C. J. Thomas, M. Monje, "Targeting neuronal activity-regulated neuroligin-3 dependency in high-grade glioma," *Nature* **549**, 533–547 (2017).
13. S. C. Buckingham, S. L. Campbell, B. R. Haas, V. Montana, S. Robel, T. Ogunrinu, H. Sontheimer, "Glutamate release by primary brain tumors induces epileptic activity," *Nat. Med.* **17**, 1269–1299 (2011).
14. S. L. Campbell, S. C. Buckingham, H. Sontheimer, "Human glioma cells induce hyperexcitability in cortical networks," *Epilepsia* **53**, 1360–1370 (2012).
15. C. C. J. Lin, K. Yu, A. Hatcher, T. W. Huang, H. K. Lee, J. Carlson, M. C. Weston, F. J. Chen, Y. Q. Zhang, W. Y. Zhu, C. A. Mohila, N. Ahnied, A. J. Patel, B. R. Arenkiel, J. L. Noebels, C. J. Creighton, B. Deneen, "Identification of diverse astrocyte populations and their malignant analogs," *Nat. Neurosci.* **20**, 396–405 (2017).
16. S. L. Campbell, S. Robel, V. A. Cuddapah, S. Robert, S. C. Buckingham, K. T. Kahle, H. Sontheimer, "GABAergic disinhibition and impaired KCC2 cotransporter activity underlie tumor-associated epilepsy," *Glia* **63**, 23–36 (2015).
17. T. Takano, J. H. C. Lin, G. Arcuino, Q. Gao, J. Yang, M. Nedergaard, "Glutamate release promotes growth of malignant gliomas," *Nat. Med.* **7**, 1010–1015 (2001).
18. Y. J. Lin, C. Y. J. Wu, J. Y. Wu, M. Lim, "The role of myeloid cells in GBM immunosuppression," *Front Immunol.* **13**, 887781 (2022).
19. C. D. Russo, N. Cappoli, "Glioma associated microglia/macrophages, a potential pharmacological target to promote antitumor inflammatory immune response in the treatment of glioblastoma," *Neuroimmunolo. Neuroinflamm.* **5**, 36 (2018).
20. C. Y. J. Wu, C. H. Chen, C. Y. Lin, L. Y. Feng, Y. C. Lin, K. C. Wei, C. Y. Huang, J. Y. Fang, P. Y. Chen, "CCL5 of glioma-associated microglia/macrophages regulates glioma migration and invasion via calcium-dependent matrix metalloproteinase 2," *Neuro Oncol.* **22**, 253–266 (2020).
21. S. F. Hussain, D. Yang, D. Suki, K. Aldape, E. Grimm, A. B. Heimberger, "The role of human glioma-infiltrating microglia/macrophages in mediating antitumor immune responses," *Neuro Oncol.* **8**, 261–279 (2006).
22. X. Z. Ye, S. L. Xu, Y. H. Xin, S. C. Yu, Y. F. Ping, L. Chen, H. L. Xiao, B. Wang, L. Yi, Q. L. Wang, X. F. Jiang, L. Yang, P. Zhang, C. Qian, Y. H. Cui, X. Zhang, X. W. Bian, "Tumor-associated microglia/macrophages enhance the invasion of glioma stem-like cells via TGF-beta1 signaling pathway," *J. Immunol.* **189**, 444–453 (2012).
23. S. Qi, H. Li, L. Lu, Z. Qi, L. Liu, L. Chen, G. Shen, L. Fu, Q. Luo, Z. Zhang, "Long-term intravital imaging of the multicolor-coded tumor microenvironment during combination immunotherapy," *Elife* **5**, e14756 (2016).

24. V. Di Nunno, E. Franceschi, A. Tosoni, L. Gatto, S. Bartolini, A. A. Brandes, "Tumor-associated microenvironment of adult gliomas: A review," *Front. Oncol.* **12**, 891543 (2022).
25. S. Qi, L. Lu, F. Zhou, Y. Chen, M. Xu, L. Chen, X. Yu, W. R. Chen, Z. Zhang, "Neutrophil infiltration and whole-cell vaccine elicited by N-dihydrogalactochitosan combined with NIR phototherapy to enhance antitumor immune response and T cell immune memory," *Theranostics* **10**, 1814–1832 (2020).
26. S. Han, C. Zhang, Q. Li, J. Dong, Y. Liu, Y. Huang, T. Jiang, A. Wu, "Tumour-infiltrating CD4(+) and CD8 (+) lymphocytes as predictors of clinical outcome in glioma," *Br. J. Cancer* **110**, 2560–2568 (2014).
27. V. Haage, M. Semtner, R. O. Vidal, D. P. Hernandez, W. W. Pong, Zh. Chen, D. Hambardzumyan, V. Magrini, A. Ly, J. Walker, E. Mardis, P. Mertins, S. Sauer, H. Kettenmann, D. H. Gutmann, "Comprehensive gene expression meta-analysis identifies signature genes that distinguish microglia from peripheral monocytes/macrophages in health and glioma," *Acta Neuropathol. Commun.* **7**, 20 (2019).
28. R. L. Bowman, F. Klemm, L. Akkari, S. M. Pyonteck, L. Sevenich, D. F. Quail, S. Dhara, K. Simpson, E. E. Gardner, C. A. Iacobuzio-Donahue, C. W. Brennan, V. Tabar, P. H. Gutin, J. A. Joyce, "Macrophage ontogeny underlies differences in glioma-specific education in brain malignancies," *Cell. Rep.* **17**, 2445–2459 (2016).
29. Z. Chen, J. L. Ross, D. Hambardzumyan, "Intravital 2-photon imaging reveals distinct morphology and infiltrative properties of glioblastoma-associated macrophages," *Proc. Natl. Acad. Sci. USA* **116**, 14254–14259 (2019).
30. S. Hernandez, F. Rojas, C. Laberiano, R. Lazcano, I. Wistuba, E. R. Parra, "Multiplex immunofluorescence tyramide signal amplification for immune cell profiling of paraffin-embedded tumor tissues," *Front Mol. Biosci.* **8**, 667067 (2021).
31. E. R. Parra, "Novel platforms of multiplexed immunofluorescence for study of paraffin tumor tissues," *J. Cancer Treat.* **2**, 43–53 (2018).
32. F. S. Varn, K. C. Johnson, J. Martinek, J. T. Huse, M. P. Nasrallah, P. Wesseling, L. A. D. Cooper, T. M. Malta, T. E. Wade, T. S. Sabedot, D. Brat, P. V. Gould, A. Woehrer, K. Aldape, A. Ismail, S. K. Sivajothi, F. P. Barthel, H. Kim, E. Kocakavuk, N. Ahmed, K. White, I. Datta, H. E. Moon, S. Pollock, C. Goldfarb, G. H. Lee, L. Garofano, K. J. Anderson, D. Nehar-Belaid, J. S. Barnholtz-Sloan, S. Bakas, A. T. Byrne, F. D'Angelo, H. K. Gan, M. Khasraw, S. Migliozzi, D. R. Ormond, S. H. Paek, E. G. Van Meir, A. M. E. Walenkamp, C. Watts, T. Weiss, M. Weller, K. Palucka, L. F. Stead, L. M. Poisson, H. Noushmehr, A. Iavarone, R. G. W. Verhaak, G. Consortium, "Glioma progression is shaped by genetic evolution and microenvironment interactions," *Cell* **185**, 2184–2199 (2022).
33. B. M. Verhoeven, S. Mei, T. K. Olsen, K. Gustafsson, A. Valind, A. Lindstrom, D. Gisselsson, S. S. Fard, C. Hagerling, P. V. Kharchenko, P. Kogner, J. I. Johnsen, N. Baryawno, "The immune cell atlas of human neuroblastoma," *Cell. Rep. Med.* **3**, 100657 (2022).
34. S. Long, Y. Zhao, Y. Xu, H. Li, H. Zhao, D. Chen, J. Zeng, H. Qiu, X. Li, Y. Gu, "Immune response induced by hematoporphyrin derivatives mediated photodynamic therapy: Immunogenic cell death and elevated costimulatory molecules," *J. Innov. Opt. Health Sci.* **15**, 2240002 (2022).
35. H. W. Ai, K. L. Hazelwood, M. W. Davidson, R. E. Campbell, "Fluorescent protein FRET pairs for ratiometric imaging of dual biosensors," *Nat. Met.* **5**, 401–403 (2008).
36. J. F. Araneda, W. E. Piers, B. Heyne, M. Parvez, R. McDonald, "High Stokes shift anilido-pyridine boron difluoride dyes," *Angew. Chem. Int. Ed. Engl.* **50**, 12214–12217 (2011).
37. E. Beurel, M. Toups, C. B. Nemeroff, "The bidirectional relationship of depression and inflammation: Double trouble," *Neuron* **107**, 234–256 (2020).
38. T. Kitabayashi, Y. Dong, T. Furuta, H. Sabit, S. Jiapaer, J. K. Zhang, G. T. Zhang, Y. Hayashi, M. Kobayashi, T. Domoto, T. Minamoto, A. Hirao, M. Nakada, "Identification of GSK3 beta inhibitor kenpaullone as a temozolomide enhancer against glioblastoma," *Sci. Rep.* **9**, 10049 (2019).
39. G. T. Zhang, S. Tanaka, S. Jiapaer, H. Sabit, S. Tamai, M. Kinoshita, M. Nakada, "RBPJ contributes to the malignancy of glioblastoma and induction of proneural-mesenchymal transition via IL-6-STAT3 pathway," *Cancer Sci.* **111**, 4166–4176 (2020).